

LECH RACZYŃSKI
WOJCIECH KRZEMIENI
KONRAD KLIMASZEWSKI

IMPROVING PET SCANNER TIME-OF-FLIGHT RESOLUTION USING ADDITIONAL PROMPT PHOTON

Abstract

Positronium Imaging requires two classes of events: double-coincidences originated from pair of back-to-back annihilation photons and triple-coincidences comprised with two annihilation photons and one additional prompt photon. The standard reconstruction of the emission position along the line-of-response of triple-coincidence event is the same as in the case of double-coincidence event; an information introduced by the high-energetic prompt photon is ignored. In this study, we propose to extend the reconstruction of position of triple-coincidence event by taking into account the time and position of prompt photon. We incorporate the knowledge about the positronium lifetime distribution and discuss the limitations of the method based on the simulation data. We highlight that the uncertainty of the estimate provided by prompt photon alone is much higher than the standard deviation estimated based on two annihilation photons. We finally demonstrate the extent of resolution improvement that can be obtained when estimated using three photons.

Keywords

positron emission tomography, positronium imaging, time resolution

1. Introduction

Positron emission tomography (PET) is a functional imaging method that is widely used in clinical oncology [1, 2, 3]. PET is used for diagnosis, staging, and monitoring treatment of cancer. The leading tracer is 18-F-fluorodeoxy-D-glucose (18-F-FDG), which helps to label tissues with high glucose uptake, such as brain, liver, kidneys, and most cancers. Together with other tomography techniques delivering morphologic and anatomic information, PET notably improves the medical diagnosis power.

State-of-the-art PET detectors focus on estimating the spatial distribution of positron emitters by measuring the two annihilation photons. These two anti-collinear photons are recorded by the pair of detectors mounted on one or more rings surrounding the patient. Detection of such event allows to identify the line-of-response (LOR) including the annihilation point. In addition to information about the LOR position, PET scanners provides also the time stamps of the arrival of the photons at the detectors. Thus for each event, time and position of annihilation may be estimated. The acquisition of a large number of LORs, typically several millions, makes it possible to reconstruct the distribution of the radiotracer injected to the patient.

However, PET may be also employed to the investigations of the local structure of the tissue via positron annihilation lifetime spectroscopy (PALS) [4, 5]. The positron history before the annihilation with an electron, not taken into consideration in the conventional PET measurement, provides the information about the tissue environment and can be useful in building the knowledge about cancer progression [6, 7, 8, 9]. It should be stressed that the positron-electron annihilation may proceed directly or via formation of positronium and the latter case occurs in tissue with probability of about 40% [10]. Positronium can exist in two states, para-positronium (p-Ps) and ortho-positronium (o-Ps) [11]. A short-lived p-Ps is formed in 25% of cases and a long-lived o-Ps in the remaining 75%. The main decay mode of p-Ps is into two photons while the o-Ps decays mostly into three photons. The self-annihilation mean lifetimes of p-Ps and o-Ps in vacuum are 125 ps and 142 ns, respectively [12]. However, in tissue, the mean lifetime of the o-Ps is reduced to about 2000 ps [6, 13] and the decay results in two photons travelling in opposite directions along the LOR, exactly as in direct annihilation. The mean value of o-Ps lifetime is sensitive to the local structure of the tissue. The relationship between the mean o-Ps lifetime and the size of molecular voids (pores) is the basis of the PALS [14]; the shortening of the mean lifetime can be translated into the radius of pore using for example Tao-Eldrup model [15].

Positronium lifetime imaging is regarded as a novel biomarker that is independent to the distribution of the radiotracer [7, 16]. This measurement requires a special class of radionuclides that apart from the positron emits also a so-called high-energetic prompt photon; lifetime of the positronium is estimated as the difference between the annihilation time and the time of the prompt photon emission. In this process it is assumed that prompt photon is emitted simultaneously in the moment of positronium formation. Lifetime imaging in human tissues relies on the acquisition of triple-coincidences comprised of the pair of back-to-back annihilation photons and the prompt photon.

In previous positronium imaging studies, the reconstruction of position of triple-coincidence event is based only on the information coming from two annihilation photons traveling along the LOR [17, 18, 19, 20, 21, 22]. In this paper, we propose to extend the position reconstruction algorithm of triple-coincidence event by taking into account additionally the time and position of prompt photon detection [23]. We will incorporate the knowledge about the positronium lifetime distribution to derive the algorithm for the position reconstruction. We will investigate the improvement of the position resolution using the additional prompt photon based on simulated PET data.

The contributions of this work are twofold: firstly, a method for reconstructing the position of triple-coincidence events is introduced and numerically validated. To the author's best knowledge, this is the first time the high-energetic prompt photon was incorporated to the determination of position along the

LOR in PET analysis. Secondly, the proposed method is compared with the reference reconstruction based on two annihilation photons only, highlighting the extent of resolution improvement obtained when estimated using three photons.

2. Standard position reconstruction

In this section we briefly describe the standard reconstruction of the emission position of triple-coincidence. State-of-the-art position reconstruction algorithm is based on times and positions of two annihilation photons only [17, 18, 21, 22]. Without loss of generality, we may rotate and shift the original 3-dimensional coordinate system into 2-dimensional local space shown in Fig. 1; the LOR marked by two annihilation photons is a green horizontal line along the x axis, and the detection positions of two annihilation photons are $(x_1, 0)$ and $(x_2, 0)$.

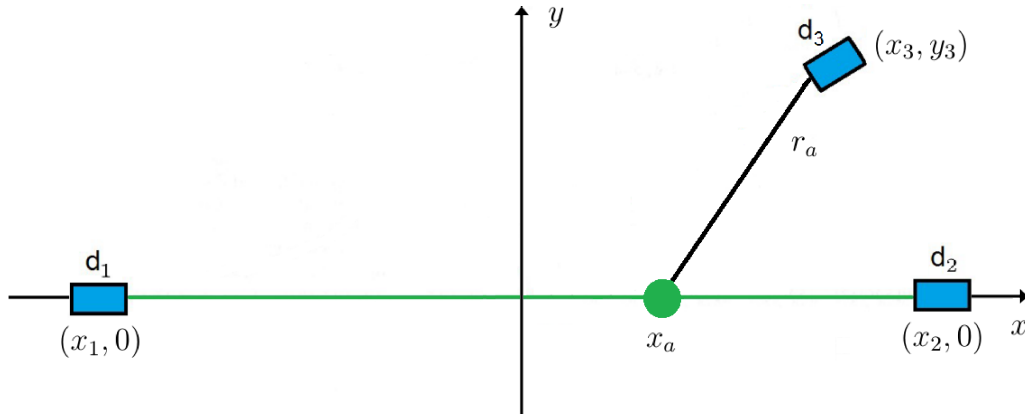


Figure 1. Position reconstruction using two annihilation photons

In this algorithm the position of the prompt photon (x_3, y_3) is ignored and the annihilation position along LOR (x_a) , marked with green circle in Fig. 1, and time (t_a) is estimated using only the information given by two annihilation photons, i.e.,

$$t_a = \frac{t_1 + t_2}{2} - \frac{|x_1 - x_2|}{2c} \quad (1)$$

$$x_a = \frac{c}{2} (t_1 - t_2) \quad (2)$$

where t_1 and t_2 are detection times in positions x_1 and x_2 , respectively, and c is the speed of light. In this work we consider only time uncertainties; times t_1, t_2, t_3 measured by detector d_1, d_2, d_3 , respectively, are noisy and the positions of detections $(x_1, 0), (x_2, 0), (x_3, y_3)$, are known exactly. We assume that time errors contributions are additive and normally distributed with standard deviation σ_t . Therefore, the standard deviations of time t_a and position x_a calculated according to Eqs 1-2 are:

$$\sigma_{t_a} = \frac{\sqrt{2}}{2} \sigma_t \quad (3)$$

$$\sigma_{x_a} = \frac{\sqrt{2}}{2} c \sigma_t. \quad (4)$$

The goal of the standard position reconstruction of triple-coincidence is to provide the information sufficient to calculate the lifetime of the positronium, i.e., parameters x_a and t_a [17, 18, 19, 20, 21, 22].

Using Eqs 1-2, first distance r_a travelled by the prompt photon from point x_a to detector d_3 is evaluated (see Fig. 1):

$$r_a = \sqrt{(x_a - x_3)^2 + y_3^2} \quad (5)$$

and then the positronium lifetime τ is estimated as:

$$\tau = t_a - t_p = t_a - t_3 + \frac{r_a}{c} \quad (6)$$

where t_p and t_3 are times of the prompt photon emission and detection, respectively.

We wish to make one comment about the uncertainties of detection times and positions. The positional uncertainty is limited to the size of the crystal and is typically of the order of a few mm. For time resolutions of state-of-the-art PET detectors, the standard deviation σ_t dominates over the standard deviation of detection position normalized by the speed of light (see Eq. 1). Therefore, in the first approximation, uncertainty along the positional dimension may be neglected during the calculations.

3. Position reconstruction based on three photons

The idea of the extended position reconstruction algorithm is to improve the uncertainty σ_{x_a} related with the estimate x_a by providing second estimate x_p marked with red circle in Fig. 2 using the prior information about prompt photon recorded in detector d_3 . The final emission position of triple-coincidence \hat{x} , marked with blue circle in Fig. 2, is found as an optimal combination of the two estimates x_a and x_p . In this section we show details of derivation of the estimate x_p and next \hat{x} .

In the standard reconstruction presented in section 2 the lifetime τ (see Eq. 6) is calculated using the distance r_a (see Eq. 5). In the extended algorithm the order of calculations is reversed: the distance $r_p \neq r_a$ travelled by the prompt photon (see Fig. 2) is evaluated based on the information about the lifetime τ . For this purpose the knowledge about prior distribution of the lifetime is required.

In recent publication [7] it was shown that the positronium lifetime τ is a random variable with probability density function (pdf):

$$\tau \sim \sum_{k=1}^3 I_k \cdot \exp\left(-\frac{t}{\lambda_k}\right). \quad (7)$$

The lifetime distribution can be represented as a three-component exponential model arising from: para-positronium annihilation (p-Ps), ortho-positronium annihilation (o-Ps) and process of direct annihilation of the positron and the electron without producing positronium. The values of lifetimes ($1/\lambda_k$) and intensities (I_k) for $k = 1, 2, 3$ are gathered in Table 1 and are based on the results presented in [7].

Table 1
Lifetime components

	Intensity (I_k)	Mean lifetime ($1/\lambda_k$)
Direct	0.65	388 ps
p-Ps	0.15	125 ps
o-Ps	0.20	2000 ps

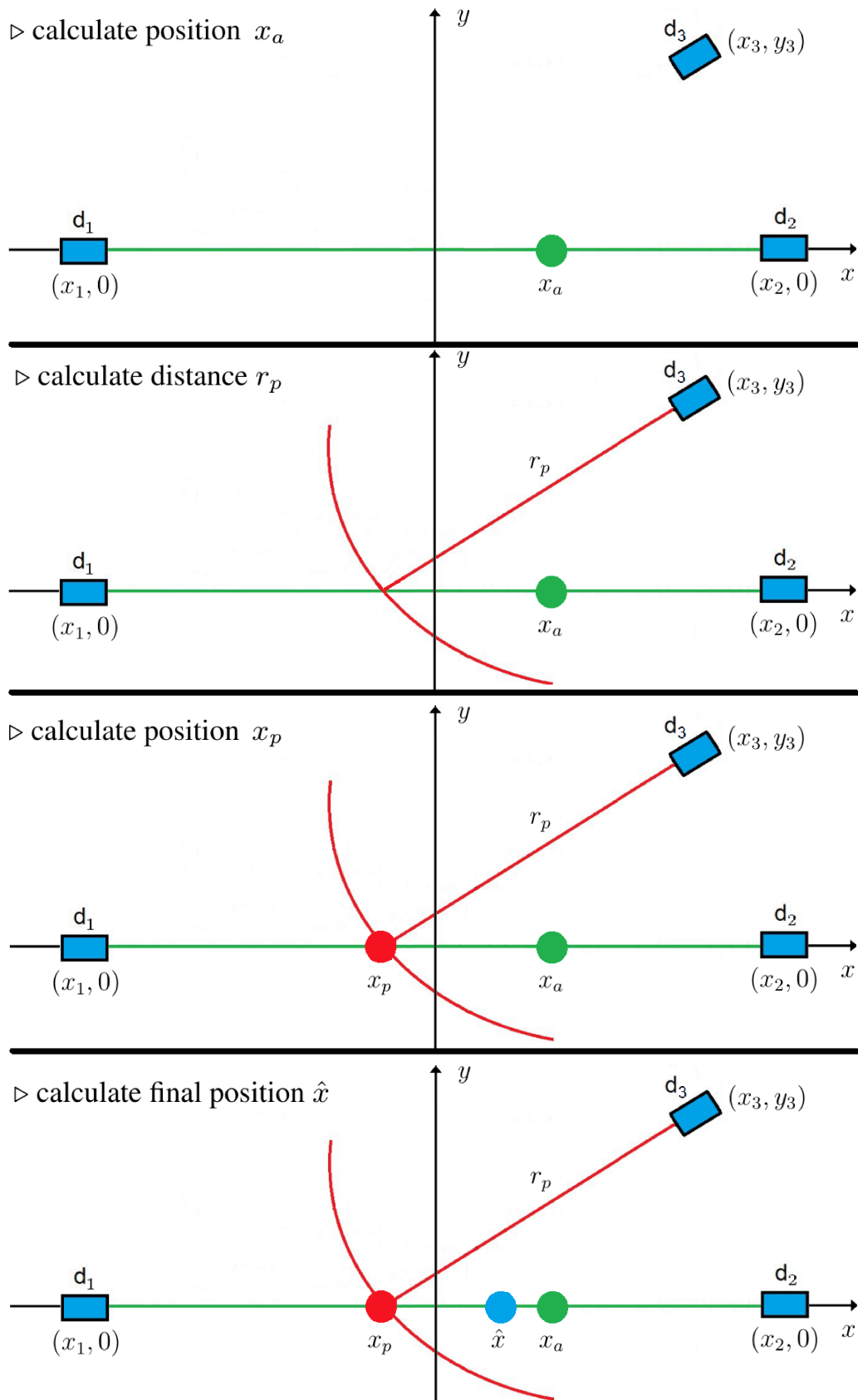


Figure 2. Position reconstruction using three photons

The distance r_p travelled by the prompt photon estimated based on the prior distribution of τ is:

$$r_p = c(t_3 - t_a + \mu_\tau) \quad (8)$$

where μ_τ is the expected value (mean value) of the lifetime distribution defined in Eq. 7. Note that in case of the proposed method, the value of the lifetime τ (see Eq. 6) is not used during the evaluation of the distance r_p in Eq. 8; we use only the expected value μ_τ . According to Eq. 8, uncertainties related with calculation of distance r_p may be modelled as a three-component exponentially modified gaussian (EMG) distributions; random variable r_p is defined as sum of two independent normal distributions (t_3 and t_a) and three-component exponential pdf (μ_τ), i.e.,

$$r_p \sim c \sum_{k=1}^3 I_k \cdot \text{EMG} \left(\frac{1}{\lambda_k}, \frac{3}{2} \sigma_t^2 \right). \quad (9)$$

In the following we will approximate the distribution of r_p with Gaussian pdf with standard deviation σ_r .

The position x_p is calculated as the intersection of the circle with center at (x_3, y_3) and radius r_p marked with red in Fig. 2 and LOR marked with green. The value of r_p greater than absolute value of y_3 guarantees that circle intersects the LOR in two points. The x_p is selected as the one whose distance from position x_a is smaller, i.e.,

$$x_p = v(r_p) = x_3 + \text{sign}(x_a - x_3) \sqrt{r_p^2 - y_3^2}. \quad (10)$$

The standard deviation σ_{x_p} of the reconstructed value x_p is evaluated using the linear term of the Taylor series of the function $v(r_p)$ in Eq. 10:

$$\sigma_{x_p} = \sigma_r \frac{r_p}{\sqrt{r_p^2 - y_3^2}}. \quad (11)$$

Finally, the estimate \hat{x} is evaluated as:

$$\hat{x} = x_a \frac{\sigma_{x_p}^2}{\sigma_{x_a}^2 + \sigma_{x_p}^2} + x_p \frac{\sigma_{x_a}^2}{\sigma_{x_a}^2 + \sigma_{x_p}^2}. \quad (12)$$

Eq. 12 shows the optimal way of combing estimates x_a and x_p with standard deviations σ_{x_a} and σ_{x_p} , respectively [24, 25, 26]. \hat{x} is the linear estimate whose standard deviation

$$\sigma_{\hat{x}} = \frac{\sigma_{x_a} \sigma_{x_p}}{\sqrt{\sigma_{x_a}^2 + \sigma_{x_p}^2}} \quad (13)$$

is less than that of any other linear combination of x_a and x_p . If σ_{x_p} were equal to σ_{x_a} , Eq. 12 says that the optimal estimate of position is simply the average of the x_a and x_p . On the other hand, if σ_{x_p} were larger than σ_{x_a} , then Eq. 12 dictates weighting x_a more heavily than x_p .

It should be stressed that in case the value of radius r_p is close to y_3 (radius of the circle in Fig. 2 would be close to perpendicular to horizontal line along x axis), the σ_{x_p} according to Eq. 11 goes to infinity, and the \hat{x} according to Eq. 12 goes to x_a . Therefore, calculation of estimate \hat{x} is reasonable only if distance:

$$r_p > |y_3| + \kappa_{\min} \sigma_r \quad (14)$$

where $\kappa_{\min} > 0$ is an additional margin.

The optimization of the value of the margin κ_{\min} will be provided during the simulation study and presented in details in section 4.2. For each triple-coincidence event the parameter κ may be calculated:

$$\kappa = \frac{r_p - |y_3|}{\sigma_r} \quad (15)$$

and the extended position reconstruction will be provided only if

$$\kappa \geq \kappa_{\min}. \quad (16)$$

Otherwise standard reconstruction of the event position using algorithm described in Section 2 is carried out. Note that the inequality in Eq. 16 is equivalent to the condition in Eq. 14. Pseudo-code of the extended algorithm of position reconstruction is presented in Algorithm 1.

Algorithm 1 Extended position reconstruction method using three photons

Require: $x_1, x_2, x_3, y_3, t_1, t_2, t_3, \sigma_{x_a}, \sigma_r, \mu_\tau, \kappa_{\min}$

- 1: $t_a \leftarrow \frac{t_1+t_2}{2} - \frac{|x_1-x_2|}{2c}$ ▷ calculate time using two annihilation photons: see Eq. 1
- 2: $x_a \leftarrow \frac{c}{2}(t_1 - t_2)$ ▷ calculate position using two annihilation photons: see Eq. 2
- 3: $r_p \leftarrow c(t_3 - t_a + \mu_\tau)$ ▷ calculate distance r_p using prior lifetime pdf: see Eq. 8
- 4: $\kappa \leftarrow \frac{r_p - |y_3|}{\sigma_r}$ ▷ calculate parameter κ : see Eq. 15
- 5: **if** $\kappa \geq \kappa_{\min}$ **then**
- 6: $x_p \leftarrow x_3 - \text{sign}(x_a - x_3) \sqrt{r_p^2 - y_3^2}$ ▷ calculate position using prompt photon alone: see Eq. 10
- 7: $\sigma_{x_p} \leftarrow \sigma_r \frac{r_p}{\sqrt{r_p^2 - y_3^2}}$ ▷ calculate standard deviation of x_p : see Eq. 11
- 8: $\hat{x} \leftarrow x_a \frac{\sigma_{x_p}^2}{\sigma_{x_a}^2 + \sigma_{x_p}^2} + x_p \frac{\sigma_{x_a}^2}{\sigma_{x_a}^2 + \sigma_{x_p}^2}$ ▷ calculate final position using three photons: see Eq. 12
- 9: $\sigma_{\hat{x}} \leftarrow \frac{\sigma_{x_a} \sigma_{x_p}}{\sqrt{\sigma_{x_a}^2 + \sigma_{x_p}^2}}$ ▷ calculate standard deviation of \hat{x} : see Eq. 13
- 10: **else**
- 11: $\hat{x} \leftarrow x_a$ ▷ calculate final position using standard algorithm
- 12: $\sigma_{\hat{x}} \leftarrow \sigma_{x_a}$ ▷ calculate standard deviation of \hat{x} using standard algorithm
- 13: **end if**

4. Results

In this section we demonstrate proof of concept of the reconstruction algorithm proposed in section 3. Sample data were generated using Monte Carlo simulation prepared in MATLAB 7.14.0 (R2012a). We modeled 2-dimensional PET scanner geometry defined as a infinitely thin cylinder with radius of 40 cm (see Fig. 3). The simulated coincidence resolving time resolution of the scanner, denoted hereafter with CRT_{ref} , was 500 ps [2, 27]. This value is defined using full width at half maximum (FWHM) as:

$$\text{CRT}_{\text{ref}} = \text{FWHM}(t_1 - t_2) \quad (17)$$

and corresponds to the standard deviation of the single time measurement in detector

$$\sigma_t \approx \frac{\text{CRT}_{\text{ref}}}{\sqrt{2} \cdot 2.35} = 150 \text{ ps}. \quad (18)$$

We simulated point sources placed in nine different radial positions in the cylinder: 0, 2, 4, 6, 8, 10, 12, 15 cm (see Fig. 3). At each position we generated in total 100,000 triple-coincidence events and reconstructed the emission point using both standard and extended algorithms presented in previous sections.

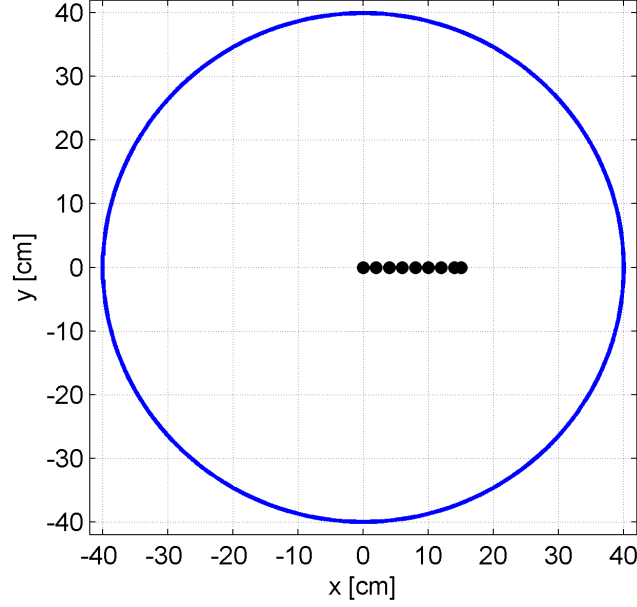


Figure 3. Simulation setup for the measurement of triple-coincidence events

In each case the value of time resolution was estimated based on the standard deviation of the position reconstruction combining Eqs 4 and 18:

$$\hat{\text{CRT}} = 2 \cdot 2.35 \cdot \frac{\sigma_{\hat{x}}}{c}. \quad (19)$$

From Eq. 19 we receive immediately that σ_{x_a} for standard position reconstruction ($\text{CRT}_{\text{ref}} = 500$ ps) is:

$$\sigma_{x_a} = \frac{\text{CRT}_{\text{ref}} \cdot c}{2 \cdot 2.35} = 3.18 \text{ cm}. \quad (20)$$

4.1. Lower bound of CRT estimated using three photons

In the first step we will derive the value of the lower bound of the time resolution of the PET detector obtained with additional information provided by the prompt photon. Substituting Eq. 13 to Eq. 19, and knowing the relation between σ_{x_a} and CRT_{ref} given in Eq. 20, we may write that:

$$\hat{\text{CRT}} = \text{CRT}_{\text{ref}} \frac{\sigma_{x_p}}{\sqrt{\sigma_{x_a}^2 + \sigma_{x_p}^2}}. \quad (21)$$

The reference value of CRT_{ref} implies directly the value of standard deviation σ_{x_a} (see Eq. 20). In the following we will show that the CRT_{ref} also has an impact on σ_{x_p} and we estimate its smallest value. Using the linear approximation of σ_{x_p} in Eq. 11 it may be shown that:

$$\sigma_{x_p} = \sigma_r \frac{r_p}{\sqrt{r_p^2 - y_3^2}} \geq \sigma_r \quad (22)$$

since

$$\frac{r_p}{\sqrt{r_p^2 - y_3^2}} \geq 1 \quad \text{for any} \quad r_p > y_3. \quad (23)$$

Substituting inequality in Eq. 22 to Eq. 21 we get the lower bound of the CRT:

$$\hat{\text{CRT}} \geq \text{CRT}_{\text{ref}} \frac{\sigma_r}{\sqrt{\sigma_{x_a}^2 + \sigma_r^2}}. \quad (24)$$

The only parameter that is missing in Eq. 24 is the standard deviation σ_r . The value of σ_r that approximates the distribution of error of distance r_p (see Eq. 9) depends on CRT_{ref} due to presence of the σ_t parameter that describes uncertainties of registration times. In this study, the evaluation of the general function of σ_r on σ_t is not crucial, and we will estimate only the value of σ_r for σ_t specified for the considered PET detector (see Eq. 18).

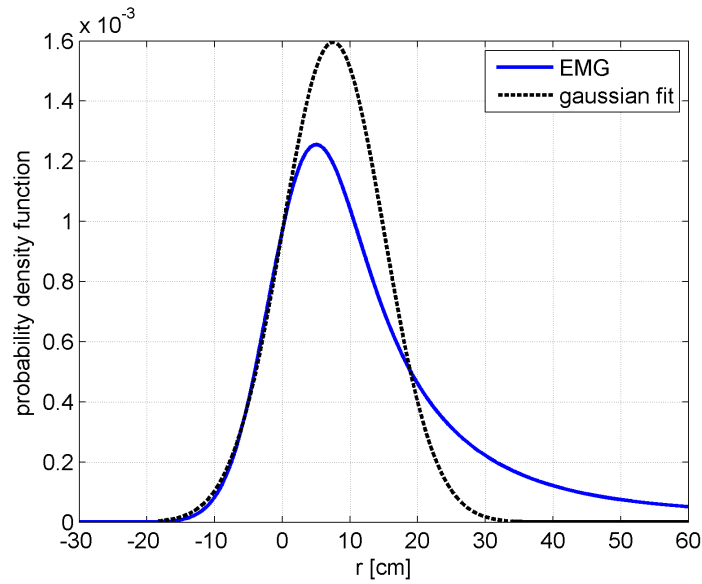


Figure 4. Approximation of the three-component EMG distribution with Gaussian fit

Theoretical pdf function of distance r_p modelled as a sum of three EMG functions according to Tab. 1, calculated for $\sigma_t = 150$ ps, is marked with blue in Fig. 4. The EMG function was calculated under the assumption that expected values of variables t_a and t_3 , given with normal distributions, are 0. It should be stressed that the EMG function is very sensitive to selected parameters of mean lifetimes and intensities (see Tab. 1). Therefore, a more general assumption about the shape of the distribution is required and in this study, a Gaussian fit was chosen. Approximation of the EMG function with normal distribution is marked with black dotted curve in Fig. 4. The parameters of the Gaussian fit are $\mu_r = 7.5$ cm and $\sigma_r = 7.5$ cm. The mean value of the Gaussian function μ_r corresponds to the mean value μ_τ of the lifetime distribution τ defined in Eq. 7. According to Eqs 8 and 9 we may write that:

$$\mu_\tau = \frac{\mu_r}{c} = 250 \text{ ps}. \quad (25)$$

Substituting the value $\sigma_r = 7.5$ cm and previous value of $\sigma_{x_a} = 3.18$ cm (see Eq. 20) to the inequality in Eq. 24 we get finally the lower bound of the CRT:

$$\hat{\text{CRT}} \geq 460 \text{ ps}. \quad (26)$$

The lower bound of the time resolution estimated using three photons is about 8% smaller than the reference value 500 ps of CRT evaluated using only two annihilation photons.

It should be stressed that there are two reasons why the lower bound CRT of about 460 ps cannot be achieved in real experiments for systems with reference 500 ps time resolution. First of all, the extended algorithm proposed in section 3 may be applied only if the condition using parameter κ in Eq. 16 is fulfilled (see line 5 in pseudo-code in Algorithm 1). Secondly, the experimental distribution of the standard deviation σ_{x_p} should be taken into account (see Eq. 21); in this section, only the smallest value of σ_{x_p} , i.e., σ_r (see Eq. 24), was analyzed. In the next step, we will derive the effective value of the CRT by considering the two remarks mentioned above and we will show that the main parameter that has the impact on the performance of the proposed algorithm is κ_{\min} .

4.2. Optimization of the reconstruction parameter κ_{\min}

In this section, we will describe the procedure of optimization of the κ_{\min} parameter and we will derive the effective value of the CRT. For this purpose, we will use the simulation data for the point source in the center of the PET scanner. First, in subsection 4.2.1 we will derive the experimental distribution of the κ parameter. Next, in subsection 4.2.2 we will introduce the dependence of the CRT on the κ parameter. Finally, in subsection 4.2.3 we will show that the κ parameter trades off between the number of the events considered in the proposed algorithm and the accuracy of the reconstruction.

4.2.1. Derivation of the cumulative distribution function of the κ parameter

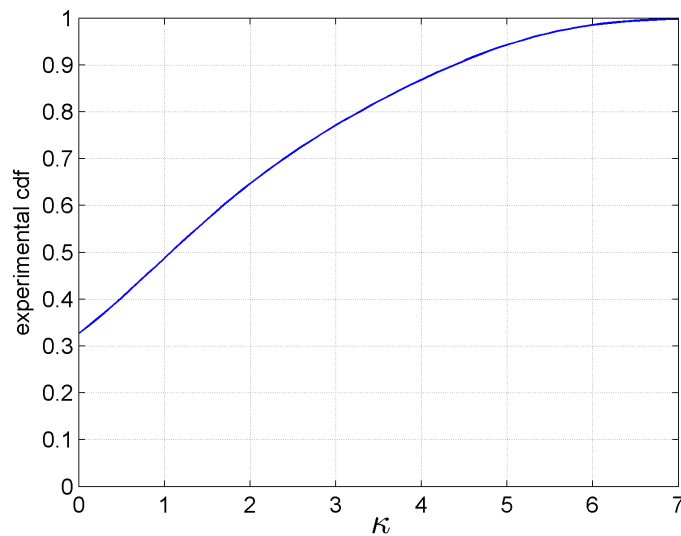


Figure 5. Cumulative distribution function of the κ parameter of the simulation data for the point source in the center of the PET detector

Using the simulation data with 100,000 triple-coincidence events we first evaluated the experimental cumulative distribution function (cdf) of the κ parameter (see Eq. 15). The resulting cdf function is shown in Fig. 5. One may see that for about 30% of events the reconstruction using the extended method is impossible since $\kappa \leq 0$. From Eq. 14 in that case the distance r_p is smaller than detection position y_3 ; circle with radius r_p has no intersections with a line marked by two annihilation photons (see Fig. 2).

Hence, in at least 30% of cases the standard position reconstruction has to be applied. The experimental cdf function for κ smaller than 0 was not presented in Fig. 5 as these values of parameter have no influence on the resulting performance of the reconstruction algorithm; in the further analysis we will investigate only positive values of the κ parameter. The highest value of κ observed in the simulation data was about 7; for this value cdf converges to 1 (see Fig. 5).

4.2.2. Investigation of dependence of the CRT on the κ parameter

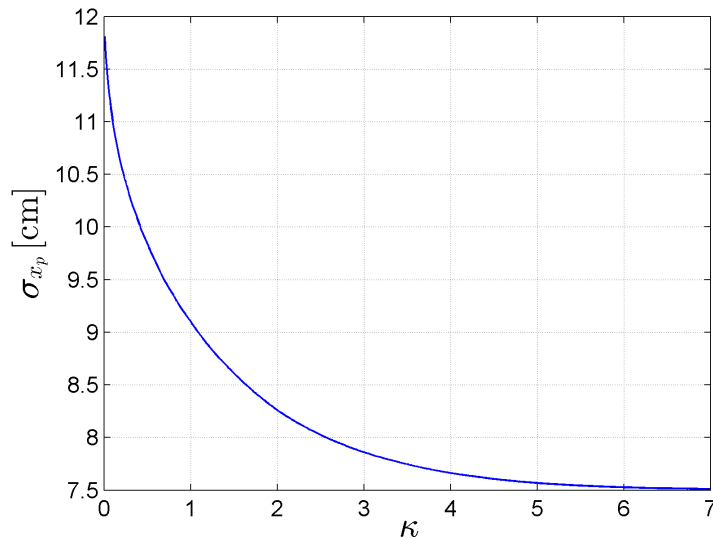


Figure 6. Mean value of the standard deviation σ_{x_p} after selecting the data based on the parameter κ

During the optimization of the κ parameter one needs to take into account that for the specified κ the mean value of the standard deviation σ_{x_p} changes. The mean value of σ_{x_p} as a function of the parameter κ is presented in Fig. 6. For a given event with the smallest considered κ close to 0, according to Eq. 11, the standard deviation σ_{x_p} goes to infinity. Therefore, in the dataset with the events with $\kappa \geq 0$ the mean value of the σ_{x_p} is the largest and is about 12 cm (see Fig. 6). Note that in that case, the largest amount of triple-coincidence events, of about 70%, may be used to position reconstruction based on extended algorithm (see the cdf function in corresponding region for $\kappa \approx 0$ in Fig. 5). Increasing the minimal value of κ from 0 to 7, one improves the mean value of standard deviation σ_{x_p} by removing the events with the worst reconstruction; the function in Fig. 6 is decreasing. It should be stressed that for $\kappa \approx 7$ the mean standard deviation σ_{x_p} converges to the value $\sigma_r = 7.5$ cm; the smallest possible value of standard deviation according to Eq. 22. However, at the same time the number of the selected events for which the proposed method may be applied also reduces and for $\kappa \approx 7$ this number goes to 0 (see the cdf function in Fig. 5). For this reason we observe the trade-off between the mean value of standard deviation σ_{x_p} and the number of triple-coincidences for which the condition using parameter κ in Eq. 14 is met.

In Fig. 7 the theoretical dependence of the scanner CRT on the mean value of the standard deviation σ_{x_p} is shown (see Eq. 21). Note that the smallest value CRT of about 460 ps corresponds to the lower bound estimated in previous section (see Eq. 26) and is estimated for $\sigma_{x_p} = \sigma_r = 7.5$ cm.

Taking into account that a given value of σ_{x_p} corresponds to the specified threshold of κ , as it was presented in Fig. 6, we have to expect that the effective value of CRT, denoted hereafter with CRT_{eff},

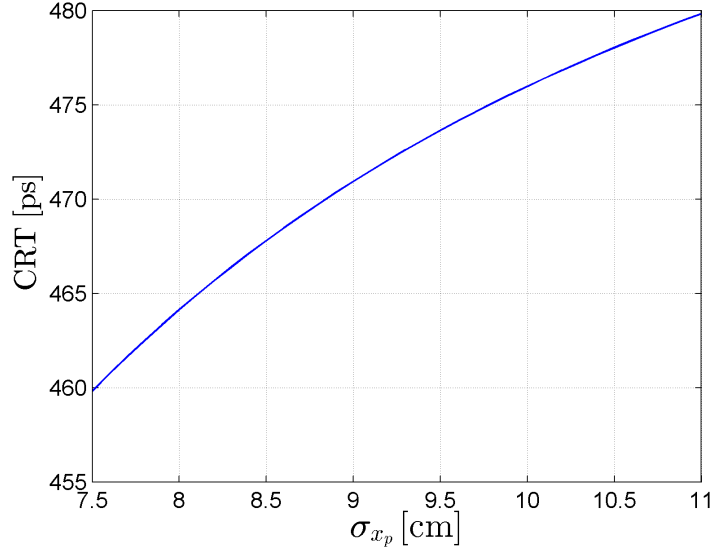


Figure 7. Dependence of the CRT on the standard deviation σ_{x_p}

will be larger than the value CRT illustrated in Fig. 7. For instance, if the threshold of the parameter κ was set to 3, from Fig. 6 we may expect that the mean value of the standard deviation σ_{x_p} in the dataset is about 7.8 cm. For this value of σ_{x_p} , from Fig. 7 we see immediately that the CRT is about 463 ps. However, this value is not the final CRT of the PET system since from Fig. 5 we may see that selection of only the events with $\kappa \geq 3$ implies that for about 77% of events the standard position reconstruction had to be applied; the effective CRT is larger than the theoretical value presented in Fig. 7. For a distinct value of the κ parameter used for selection criteria, a different effective value of the time resolution will be obtained.

4.2.3. Final optimization of the reconstruction parameter κ_{\min}

The problem of finding the smallest effective resolution time (CRT_{eff}) is equivalent to the optimization task of the κ parameter. For this purpose, we need to recall the definition of the standard deviation calculated using two reconstructions x_a (standard algorithm see Eq. 2) and \hat{x} (extended algorithm see Eq. 12):

$$\sigma_{x_{\text{eff}}}^2 = \frac{1}{N_a + \hat{N}} \left(\sum_i^{N_a} (x_a(i) - m)^2 + \sum_j^{\hat{N}} (\hat{x}(j) - m)^2 \right). \quad (27)$$

In Eq. 27 values N_a and \hat{N} denote the numbers of the triple-coincidence events for which the standard and the extended reconstruction methods were applied, respectively. In other words, in N_a cases the calculated value of κ was smaller than the selected threshold and for the remaining \hat{N} cases the parameter κ was higher than the threshold. We assumed that both methods are unbiased, and the same mean value

of the position reconstruction m is obtained. Taking into account that:

$$\sigma_{x_a}^2 = \frac{1}{N_a} \sum_i^{N_a} (x_a(i) - m)^2 \quad (28)$$

$$\sigma_{\hat{x}}^2 = \frac{1}{\hat{N}} \sum_j^{\hat{N}} (\hat{x}(j) - m)^2 \quad (29)$$

based on Eq. 27 we may write that:

$$\sigma_{x_{\text{eff}}}^2 = \frac{1}{N_a + \hat{N}} (N_a \sigma_{x_a}^2 + \hat{N} \sigma_{\hat{x}}^2). \quad (30)$$

The effective value of the CRT calculated using Eq. 30 and based on previous derivations of σ_{x_a} and $\sigma_{\hat{x}}$ in Eqs 20 and 19, respectively, is given as:

$$\text{CRT}_{\text{eff}} = \sqrt{\frac{N_a}{N_a + \hat{N}} \text{CRT}_{\text{ref}}^2 + \frac{\hat{N}}{N_a + \hat{N}} \hat{\text{CRT}}^2}. \quad (31)$$

Fig. 8 presents the relation between the CRT_{eff} and the value of the selected κ parameter. The parameter κ trades off the number of the events considered in the proposed algorithm and the accuracy of the reconstruction. Large values of the parameter favor triple-coincidence events with best position resolution. For κ about 7 no events meet the condition in Eq. 14 and the effective CRT converges to the reference value of time resolution of 500 ps. Decreasing the value of κ tends to improve the performance of the reconstruction. The smallest $\text{CRT}_{\text{eff}} \approx 486$ ps is observed for κ about 0.7. For smaller values of κ the time resolution starts to increase.

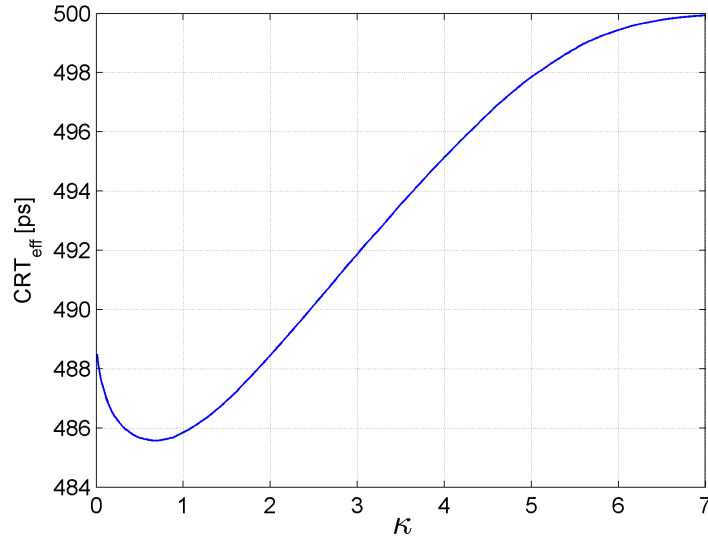


Figure 8. Calculation of the effective CRT as the function of κ parameter

4.3. Simulation study of estimation of CRT using three photons

In the last part of this study, we will derive the effective value of the CRT in different radial positions of the PET scanner based on the simulation data. We will also compare the values of CRT estimated using the proposed scheme and the reference method. During the comparative study presented in this section we applied the threshold $\kappa_{\min} = 0.7$ based on the results shown in Fig. 8. This requirement imposes that the extended position reconstruction method uses about 55% of acquired triple-coincidence events (see Fig. 5). For the estimation of the position in remaining 45% of cases only the information from two annihilation photons was taken into account; in that case the resulting positions for both compared methods are the same.

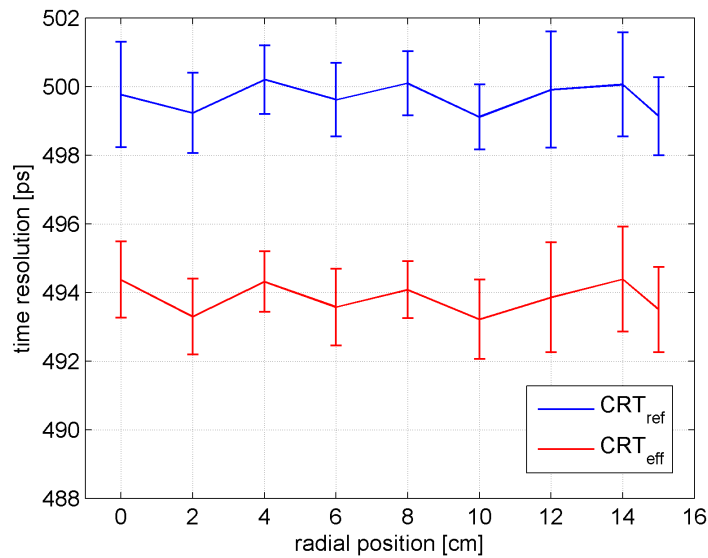


Figure 9. Calculation of the CRT using two reconstruction methods: standard (blue curve), extended (red curve)

Fig. 9 compares the time resolutions of the PET scanner calculated in different radial positions using two methods: reference reconstruction algorithm (blue curve) and proposed reconstruction algorithm (red curve). The error bars indicate standard deviations and were estimated from the 10 realizations of event smearing with assumed resolution of 500 ps. The evaluation of the distribution of the CRT for the reference method (CRT_{ref}) was performed only for validation purposes; as expected the resulting curve is stable at the level of 500 ps. The effective value of the time resolution estimated using the proposed scheme (CRT_{eff}) is on average about 494 ps and is slightly better than the CRT_{ref} . The experimental value of CRT_{eff} for center position is about 8 ps higher than the theoretical one for $\kappa_{\min} = 0.7$ shown in Fig. 8.

5. Conclusions

In this article, the extended method for position reconstruction of the triple-coincidence event was introduced. The key feature of this model is the incorporation of knowledge about the time and position of prompt photon detection. We have evaluated the lower bound of the coincidence resolving time resolution for the proposed method and we have shown that this value is about 8% smaller in comparison to the reference scanner CRT of 500 ps. We highlighted the statistical phenomenon that deteriorates the quality of

the reconstruction: the uncertainty of the estimate provided by prompt photon alone (σ_{x_p}) is much higher than the standard deviation of the reference model (σ_{x_a}). This leads to (1) decreasing the quality of the estimate based on both reconstructions and (2) excluding a fraction of the events with the worst predicted uncertainty from the proposed reconstruction framework. We have optimized the main parameter κ_{\min} of the model that trades off the number of the events considered in the proposed algorithm and the accuracy of the reconstruction. Finally, the effective value of the estimated CRT was about 494 ps and was only slightly better than the reference time resolution of the PET scanner.

Future work will investigate other aspects of signal processing by using the proposed statistical model, for instance, the influence of the reference value of the scanner CRT on the effective time resolution. In this study, the time resolution of the detector system of 500 ps was assumed. However, recent theoretical and experimental studies using small scintillator crystals indicate that the CRT limit is expected at about 100 ps [28, 29]. In the next steps, we plan to investigate the potential position reconstruction improvement for the systems with CRT smaller than 500 ps.

References

- [1] Karp J., Surti S., Daube-Witherspoon M., Muehllehner G.: Benefit of Time-of-Flight in PET: Experimental and Clinical Results. In: *Journal of Nuclear Medicine*, vol. 49, pp. 462–470, 2008. URL <http://dx.doi.org/10.2967/jnumed.107.044834>.
- [2] Słomka P., Pan T., Germano G.: Recent advances and future progress in PET instrumentation. In: *Semin. Nucl. Med.*, vol. 46, pp. 5–19, 2016. URL <http://dx.doi.org/10.1053/j.semnuclmed.2015.09.006>.
- [3] Conti M., Bendriem B.: The new opportunities for high time resolution clinical TOF PET. In: *Clin. Trans. Imag.*, vol. 7, pp. 139–147, 2019. URL <http://dx.doi.org/10.1007/s40336-019-00316-5>.
- [4] Jasinska B., Zgardzinska B., Cholubek G., Gorgol M., Wiktor K., Wysoglad K., Bialas P., Curceanu C., Czerwinski E., Dulski K., Gajos A., Glowacz B., Hiesmayr B., Jodlowska-Jedrych B., Kaminska D., Korcyl G., Kowalski P., Kozik T., Krawczyk N., Krzemień W., Kubicz E., Mohammed M., Pawlik-Niedzwiecka M., Niedzwiecki S., Palka M., Raczynski L., Rudy Z., Sharma N., Sharma S., Shopa R., Silarski M., Skurzok M., Wieczorek A., Wiktor H., Wislicki W., Zielinski M., Moskal P.: Human Tissues Investigation Using PALS Technique. In: *Acta Physica Polonica B*, vol. 48, p. 1737, 2017. URL <http://dx.doi.org/10.5506/APhysPolB>.
- [5] Jasinska B., Zgardzinska B., Cholubek G., Pietrow M., Gorgol M., Wiktor K., Wysoglad K., Bialas P., Curceanu C., Czerwinski E., Dulski K., Gajos A., Glowacz B., Hiesmayr B., Jodlowska-Jedrych B., Kaminska D., Korcyl G., Kowalski P., Kozik T., Krawczyk N., Krzemień W., Kubicz E., Mohammed M., Pawlik-Niedzwiecka M., Niedzwiecki S., Palka M., Raczynski L., Rudy Z., Sharma N., Sharma S., Shopa R., Silarski M., Skurzok M., Wieczorek A., Wiktor H., Wislicki W., Zielinski M., Moskal P.: Human Tissue Investigations Using PALS Technique - Free Radicals Influence. In: *Acta Physica Polonica A*, vol. 132, p. 1556, 2017. URL <http://dx.doi.org/10.12693/APhysPolA.132.1556>.
- [6] Shibuya K., Saito H., Nishikido F., Takahashi M., Yamaya T.: Oxygen sensing ability of positronium atom for tumor hypoxia imaging. In: *Communications Physics*, vol. 3, p. 173, 2020. URL <http://dx.doi.org/10.1038/s42005-020-00440-z>.
- [7] Moskal P., Dulski K., Chug N., Curceanu C., Czerwinski E., Dadgar M., Gajewski J., Gajos A., Grudzien G., Hiesmayr B., Kacprzak K., Kaplon L., Karimi H., Klimaszewski K., Korcyl G., Kowalski P., Kozik T., Krawczyk N., Krzemień W., Kubicz E., Malczak P., Pawlik-Niedzwiecka M., Niedzwiecki S., Pedziwiatr M., Raczynski L., Raj J., Rucinski A., Sharma S., Shivani S., Shopa

- R., Silarski M., Skurzok M., Stepień E., Szczepanek M., Tayefi F., Wislicki W.: Positronium imaging with the novel multiphoton PET scanner. In: *Science Advances*, vol. 7, p. 4394, 2021. URL <http://dx.doi.org/10.1126/sciadv.abh4394>.
- [8] Steinberger W., Mercolli L., Breuer J., Sari H., Parzych S., Niedzwiecki S., Lapkiewicz G., Moskal P., Stepień E., Rominger A., Shi K., Conti M.: Positronium lifetime validation measurements using a long-axial field-of-view positron emission tomography scanner. In: *EJNMMI Physics*, vol. 11, p. 76, 2024. URL <http://dx.doi.org/10.1186/s40658-024-00678-4>.
- [9] Moskal P., Baran J., Bass S., Choinski J., Chug N., Curceanu C., Czerwinski E., Dadgar M., Das M., Dulski K., Eliyan K., Fronczewska K., Gajos A., Kacprzak K., Kajetanowicz M., Kaplanoglu T., Kaplon L., Klimaszewski K., Kobylecka M., Korcyl G., Kozik T., Krzemien W., Kubat K., Kumar D., Kunikowska J., Maczewska J., Migdal W., Moskal G., Mryka W., Niedzwiecki S., Parzych S., Perez del Rio E., Raczynski L., Sharma S., Shivani S., Shopa R., Silarski M., Skurzok M., Tayefi F., Tayefi K., Tanty P., Wislicki W., Krolicki L., Stepień E.: Positronium image of the human brain in vivo. In: *Science Advances*, vol. 10, p. 1, 2024. URL <http://dx.doi.org/10.1126/sciadv.adp2840>.
- [10] Bass S., Mariazzi S., Moskal P., E. S.: Colloquium: Positronium physics and biomedical applications. In: *Rev. Mod. Phys.*, vol. 95, p. 021002, 2023. URL <http://dx.doi.org/10.1103/RevModPhys.95.021002>.
- [11] Harpen M.: Positronium: Review of symmetry, conserved quantities and decay for the radiological physicist. In: *Medical Physics*, vol. 31, pp. 57–61, 2003. URL <http://dx.doi.org/10.1118/1.1630494>.
- [12] Cassidy D.: Experimental progress in positronium laser physics. In: *European Physical Journal D*, vol. 72, p. 53, 2018. URL <http://dx.doi.org/10.1140/epjd/e2018-80721-y>.
- [13] Jasinska B., Moskal P.: A New PET Diagnostic Indicator Based on the Ratio of 3 gamma to 2 gamma Positron Annihilation. In: *Acta Physica Polonica B*, vol. 48, p. 1577, 2017. URL <http://dx.doi.org/10.5506/APhysPolB.48.1577>.
- [14] Zgardzinska B., Cholubek G., Jarosz B., Wysoglad K., Gorgol M., Gozdzik M., Cholubek M., Jasinska B.: Studies on healthy and neoplastic tissues using positron annihilation lifetime spectroscopy and focused histopathological imaging. In: *Scientific Reports*, vol. 10, p. 11890, 2020. URL <http://dx.doi.org/10.1038/s41598-020-68727-3>.
- [15] Tao S.: Positronium Annihilation in Molecular Substances. In: *J. Chem. Phys.*, vol. 56, pp. 5499–5510, 1972. URL <http://dx.doi.org/10.1063/1.1677067>.
- [16] Takyu S., Nishikido F., Tashima H., Akamatsu G., Matsumoto K., Takahashi M., Yamaya T.: Positronium lifetime measurement using a clinical PET system for tumor hypoxia identification. In: *Nuclear Instruments and Methods in Physics Research Section A: Accelerators, Spectrometers, Detectors and Associated Equipment*, vol. 1065, p. 169514, 2024. URL <http://dx.doi.org/10.1016/j.nima.2024.169514>.
- [17] Shopa R., Dulski K.: Multi-photon time-of-flight MLEM application for the positronium imaging in J-PET. In: *Bio-Algorithms and Med-Systems*, vol. 18, p. 135, 2022. URL <http://dx.doi.org/10.2478/bioal-2022-0082>.
- [18] Shopa R., Dulski K.: Positronium imaging in J-PET with an iterative activity reconstruction and a multi-stage fitting algorithm. In: *Bio-Algorithms and Med-Systems*, vol. 19, p. 54, 2023. URL <http://dx.doi.org/10.5604/01.3001.0054.1826>.
- [19] Shibuya K., Saito H., Tashima H., Yamaya T.: Using inverse Laplace transform in positronium lifetime imaging. In: *Physics in Medicine and Biology*, vol. 67, p. 025009, 2022. URL <http://dx.doi.org/10.1088/1361-6560/ac499b>.

- [20] Jegal J., Jeong D., Seo E., Park H., Kim H.: Convolutional neural network-based reconstruction for positronium annihilation localization. In: *Scientific Reports*, vol. 12, p. 8531, 2022. URL <http://dx.doi.org/10.1038/s41598-022-11972-5>.
- [21] Qi J., Huang B.: Positronium lifetime image reconstruction for TOF PET. In: *IEEE Transactions on Medical Imaging*, vol. 41, p. 2848, 2022. URL <http://dx.doi.org/10.1109/TMI.2022.3174561>.
- [22] Huang B., Li T., Arino-Estrada G., Dulski K., Shopa R., Moskal P., Stepien E., Qi J.: Split: Statistical positronium lifetime image reconstruction via time-thresholding. In: *IEEE Transactions on Medical Imaging*, vol. 43, p. 2148, 2024. URL <http://dx.doi.org/10.1109/TMI.2024.3357659>.
- [23] Giovagnoli D., Bousse A., Beaupere N., Canot C., Cussonneau J., Diglio S., Carreres A., Masbou J., Merlin T., Morteau E., Xing Y., Zhu Y., Thers D., Visvikis D.: A Pseudo-TOF Image Reconstruction Approach for Three-Gamma Small Animal Imaging. In: *IEEE Transactions on Radiation and Plasma Medical Sciences*, vol. 5, pp. 826–834, 2020. URL <http://dx.doi.org/10.1109/TRPMS.2020.3046409>.
- [24] Kalman R.: A New Approach to Linear Filtering and Prediction Problems. In: *Transaction of the ASME-Journal of Basic Engineering*, pp. 35–45, 1960.
- [25] Sorenson H.: Least-Squares estimation: from Gauss to Kalman. In: *IEEE Spectrum*, vol. 7, pp. 63–68, 1970.
- [26] Jacobs O.: *Introduction to Control Theory*. Oxford University Press, 1993.
- [27] van Sluis J., de Jong J., Schaar J., Noordzij W., van Snick P., Dierckx R., Borra R., Willemsen A., Boellaard R.: Performance Characteristics of the Digital Biograph Vision PET/CT System. In: *Journal of Nuclear Medicine*, vol. 60, pp. 1031–1036, 2019. URL <http://dx.doi.org/10.2967/jnumed.118.215418>.
- [28] Schaart D., Seifert S., Vinke R., van Dam H., Dendooven P., Lohner H., Beekman F.: LaBr₃: Ce and SiPMs for time-of-flight PET: achieving 100 ps coincidence resolving time. In: *Physics in Medicine and Biology*, vol. 55, pp. N179–89, 2010. URL <http://dx.doi.org/10.1088/0031-9155/55/7/N02>.
- [29] Cates J., Levin C.: Evaluation of a clinical TOF-PET detector design that achieves less than 100 ps coincidence time resolution. In: *Physics in Medicine and Biology*, vol. 63, p. 115011, 2018. URL <http://dx.doi.org/10.1088/1361-6560/aac504>.

Affiliations

Lech Raczyński

Department of Complex Systems, National Centre for Nuclear Research, 05-400 Otwock-Swierk, Poland,
lech.raczynski@ncbj.gov.pl

Wojciech Krzemień

High Energy Physics Division, National Centre for Nuclear Research, 05-400 Otwock-Swierk, Poland,
wojciech.krzemien@ncbj.gov.pl

Konrad Klimaszewski

Department of Complex Systems, National Centre for Nuclear Research, 05-400 Otwock-Swierk, Poland,
konrad.klimaszewski@ncbj.gov.pl

Received: ???

Revised: ???

Accepted: ???